JACS
JOURNAL OF THE AMERICAN CHEMICAL SOCIETY
Communication
pubs.acs.org/JACS

Nitrite Activation to Nitric Oxide via One-fold Protonation of Iron(II)-*O,O*-nitrito Complex: Relevance to the Nitrite Reductase Activity of Deoxyhemoglobin and Deoxyhemerythrin

Chih-Chin Tsou, Wan-Lin Yang, and Wen-Feng Liaw*

Department of Chemistry and Frontier Research Center on Fundamental and Applied Sciences of Matters, National Tsing Hua University, Hsinchu, 30013, Taiwan

Supporting Information

ABSTRACT: The reversible transformations $[(Bim)_3Fe(\kappa^2\text{-}O_2N)][BF_4]$ (**3**) ⇌ $[(Bim)_3Fe(NO)(\kappa^1\text{-}ONO)][BF_4]_2$ (**4**) were demonstrated and characterized. Transformation of *O,O*-nitrito-containing complex **3** into $[(Bim)_3Fe(\mu\text{-}O)(\mu\text{-}OAc)Fe(Bim)_3]^{3+}$ (**5**) along with the release of NO and H_2O triggered by 1 equiv of AcOH implicates that nitrite-to-nitric oxide conversion occurs, in contrast to two protons needed to trigger nitrite reduction producing NO observed in the protonation of [Fe^{II}-nitro] complexes.

Nitrite, a ubiquitous molecule in vivo and, particularly, in the endocrine system has been known to serve as an intravascular NO storage/transport species to transduce NO bioactivity in blood circulation. Nitrite signaling operates through the cooperative action with hemes, thiols, amines, polyphenols, and ascorbate yielding nitric oxide during physiological and pathological hypoxia.[1] In biological system and chemistry, coordination of nitrite to monometallic center displays three types of binding mode: metal-*N*-nitro (M-κ^1-NO_2), metal-*O*-nitrito (M-κ^1-ONO), and metal-*O,O*-nitrito (M-κ^2-O_2N).[2,3] The heme-nitrite binding modes [heme-Fe^{III}-nitro], [heme-Fe^{III}-nitro/-*O*-nitrito], and [heme-Fe^{III}-*O*-nitrito] have been structurally characterized in the bacterial nitrite reductases (NiR) from *P. pantotrophus*/*W. succinogenes*,[3] horse myoglobin (Mb),[4,5] and human hemoglobin (Hb),[3,6] respectively. Of importance, the reaction of deoxyhemoglobin and nitrite under hypoxic conditions producing nitrosylhemoglobin was demonstrated to vasodilate circulation and increase blood flow before and during exercise.[7] In protonation of heme-nitrite yielding NO, the electrophilic attack of two protons on the O atom of heme-nitro resulting in the formation of water and an intermediate $\{Fe(NO)\}^6$ species, eventually releasing NO (Chart 1a), and only one hydrogen-bonding interaction participating in the O_{endo} atom of heme-*O*-nitrito leading to the formation of a hydroxyl ferric complex and NO were supported by crystallography,[3−6] rate constant studies,[7−9] and DFT computations (Chart 1b).[10] The latter-type reaction has not yet been experimentally characterized in model chemistry. In non-heme systems, the [4Fe-4S] cluster in *C. botulinum* was observed to transform into dinitrosyl iron complexes (DNICs) under the incubation of nitrite.[11] The high concentration of dimeric DNICs $[(\mu\text{-}SMe)Fe(NO)_2]_2$ was characterized in pickled cabbages under treatment of $NaNO_2$.[12,13] Interestingly, we notice that nitrosylation of deoxyhemerythrin by nitrite under pH 6.3−7.5 buffer yielding semi-met nitrosyl adduct and hydroxide was also reported via 1-fold protonation.[14]

In model chemistry, as shown in Scheme 1, nitrite activation producing NO triggered by iron complexes can be classified into the following types: (a) thioether-/thiol-triggered oxygen-atom-transfer (OAT) of [porphyrin-Fe^{III}-nitro],[15−17] (b) 2-fold (double) protonation of [N-confused porphyrin-Fe^{II}-nitrite],[18] (c) PPh_3-triggered OAT of [L_1-Fe^{III}-nitro] (L_1 = $N(CH_2$-2-

Chart 1

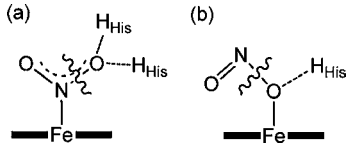

Scheme 1. Nitrite Reduction by Heme and Non-Heme Iron Model Complexes[a]

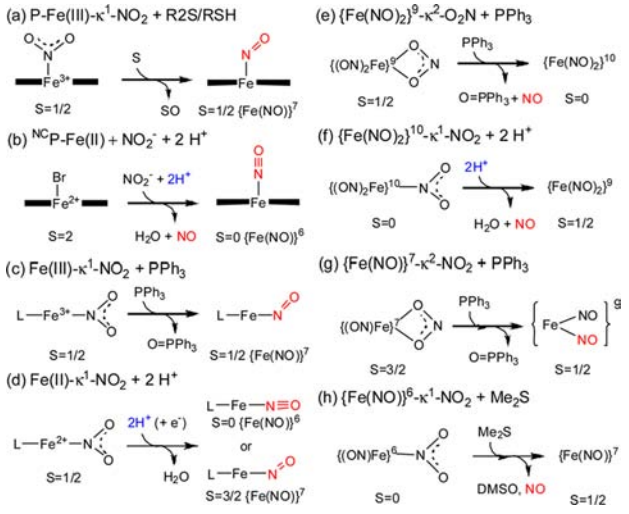

[a]P = porphyrin; NCP = N-confused porphyrin. Feltham-Enemark notation $\{Fe(NO)_x\}^n$ (*n* denotes as sum of electrons of the metal d orbitals and NO π^* orbitals).[24]

Received: October 16, 2013
Published: December 1, 2013

dx.doi.org/10.1021/ja4105864 | J. Am. Chem. Soc. 2013, 135, 18758−18761

$C_5H_4N)_2(CH_2$-$CH_2NC(O)$-2-$C_5H_4N)$ or 1,2-$C_6H_4(NC(O)$-2-$C_5H_4N)_2$),[19,20] (d) 2-fold protonation of [L_2-Fe^{II}-nitro] (L_2 = $N(CH_2CH_2NH_2)_2$-$(CH_2CH_2N{=}C(CH_3)C(CH_3)_2S$ or 2,6-$C_5H_3N[CMe(CH_2{-}NH_2)_2]_2$),[21−23] (e) PPh_3-triggered OAT of $\{Fe(NO)_2\}^9$ DNIC [$(NO)_2$Fe-*O*,*O*-nitrito],[25] (f) 2-fold protonation of $\{Fe(NO)_2\}^{10}$ DNIC [$(NO)_2$Fe-nitro],[26] (g) PPh_3-triggered OAT of MNIC $\{Fe(NO)\}^7$ [(NO)Fe-*O*,*O*-nitrito],[26] and (h) Me_2S-triggered OAT of MNIC $\{Fe(NO)\}^6$ [(NO)Fe-nitro].[27] In this report, a ferrous-*O*,*O*-bound nitrito model complex $[(Bim)_3Fe(\kappa^2\text{-}O_2N)]^+$ ($(Bim)_3$ = tris(2-benzimidazolylmethyl)amine)[28] (**3**) was synthesized. Complex **3** was demonstrated to react with 1 equiv of acetic acid to produce nitric oxide along with the formation of diferric-oxo complex $[(Bim)_3Fe(\mu\text{-}O)(\mu\text{-}OAc)Fe(Bim)_3]^{3+}$ (**5**) and H_2O. This result provides the first Fe-mediated nitrite activation yielding $NO_{(g)}$ via 1-fold protonation of [Fe^{II}-*O*,*O*-nitrito] model complex.

$[(Bim)_3Fe(MeCN)][BF_4]_2$ (**1**) was synthesized from the reaction of $[Fe(H_2O)_6][BF_4]_2$ and $(Bim)_3$ in MeCN at room-temperature. The local geometry of complex **1** exhibits a distorted trigonal bipyramidal (τ = 0.90) (Supporting Information (SI) Figure S1). The effective magnetic moment (μ_{eff}) of complex **1** in the solid state at 300 K is 4.97 μ_B, indicating a S = 2 ground state (SI Figure S2). Reaction of complex **1** and 1 equiv of $NO_{(g)}$ led to the formation of $\{Fe(NO)\}^7$ $[(Bim)_3Fe(NO)][BF_4]_2$ (**2**), characterized by IR (ν_{NO}: 1814 s cm^{-1} (MeCN)), UV−vis, ^1H NMR spectroscopies, and single-crystal X-ray diffraction (XRD) (SI Figures S3−S5). The Fe−N (1.731(6) Å) and N−O (1.156(7) Å) bond distances fall in the range of 1.659(6) to 1.779(9) Å (Fe−N(O)) and 1.002(9) to 1.193(4) Å (N−O) observed in the $\{Fe(NO)\}^7$ mononitrosyl iron complexes (MNICs).[27] Interestingly, MNIC **2** dissolved in MeCN readily releases $NO_{(g)}$ under vacuum to reform complex **1**.

Addition of 2 equiv of $NaNO_2$ into complex **1** in THF yielded $[(Bim)_3Fe(\kappa^2\text{-}O_2N)][BF_4]$ (**3**), identified by IR, UV−vis, ^1H NMR spectroscopies, and single-crystal XRD (Experimental Section, SI Figures S6, S7 and Figure 1a). The Fe−O bond distances (2.104(4) and 2.338(4) for Fe(1)−O(1) and Fe(1)−O(2), respectively) indicate complex **3** contains an asymmetric *O*,*O*-bound nitrito ligand (Figure 1a). The IR spectra of complex **3** display ν_{O-N-O} stretching frequency at 1277 cm^{-1} ($\nu_{O-^{15}N-O}$ 1263 cm^{-1} (KBr), SI Figure S8). The temperature-dependent μ_{eff} values decrease from 5.08 μ_B at 300 K to 4.20 μ_B at 2 K, which are close to the spin-only value (μ_{eff} = 4.90 μ_B) for a high-spin S = 2 system (SI Figure S9). In contrast to the reaction of $[(pyN_4)Fe^{II}Br]^+$ (S = 2) (pyN_4 = 2,6-$C_5H_3N[CMe(CH_2NH_2)_2]_2$) and nitrite yielding diamagnetic $[(pyN_4)Fe^{II}(\kappa^1\text{-}NO_2)]^+$,[23] the reaction of complex **1** and nitrite produces a paramagnetic complex **3** with S = 2. The differences of nitrite binding modes and magnetic properties between $[(pyN_4)Fe^{II}(\kappa^1\text{-}NO_2)]^+$ and complex **3** may be attributed to the different electron-donating ability of pyN_4 and $(Bim)_3$ coordinate ligands. The pyN_4-coordinate ligand of $[(pyN_4)Fe(\kappa^1\text{-}NO_2)]^+$ donates more electron density, compared to $(Bim)_3$ ligand of complex **3**, to lead to N-bound nitro species. Presumably, *O*,*O*-bound chelating nitrito acts as a σ donor ligand in complex **3**.

Of importance, addition of 1 equiv of NO(g) into the MeCN solution of complex **3** yielded six-coordinate $\{Fe(NO)\}^7$ $[(Bim)_3Fe(NO)(\kappa^1\text{-}ONO)][BF_4]$ (**4**), characterized by IR (ν_{NO}: 1791 cm^{-1} (MeCN); 1770 cm^{-1} (KBr)), UV−vis, ^1H NMR spectroscopies and XRD (Scheme 2; SI Figures S10−S12 and Figure 1b). Upon addition of NO into $[(Bim)_3Fe(\kappa^2\text{-}O_2{}^{15}N)][BF_4]$, the appearance of 1770 cm^{-1} (ν_{NO}) and 1735 cm^{-1} ($\nu^{15}{}_{NO}$) (KBr) stretching frequencies corroborated isotopic scrambling between $[\kappa^1\text{-}O^{15}NO]^-$ and NO in complex **4** (SI Figure S10). The Fe−N (1.731(6) Å) and N−O (1.156(7) Å) bond distances also fall in the range of Fe−N(O) and N−O bond lengths observed in the $\{Fe(NO)\}^7$ MNICs (Figure 1b).[27] Compared to the liberation of NO of MNIC **2** under vacuum, the nitrosyl group in MNIC **4** is easier to liberate to reform complex **3** under vacuum via nitrite chelation.

Scheme 2. Reaction of Complex 3 and AcOH Leads to the Formation of Complex 5 along with the Release of NO(g) and H_2O

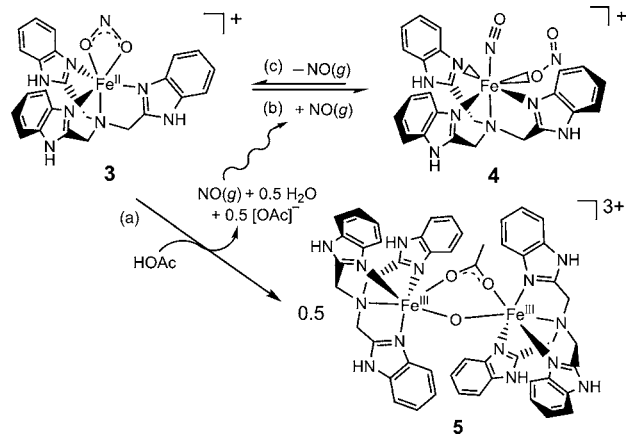

In order to characterize the electronic structures of $\{Fe(NO)\}^7$ MNICs **2** and **4**, EPR and SQUID measurements were carried out. The EPR spectra of complexes **2** and **4** in MeCN at 4 K display slight rhombic S = 3/2 signals (g_1 = 4.066, g_2 = 3.876, g_3 = 1.995 for **2**; g_1 = 4.045, g_2 = 3.885, g_3 = 1.996 for **4**), which is best fitted by using parameters $\mathbf{g_e}$ = 1.980 and E/D = 0.010 for **2** and $\mathbf{g_e}$ = 1.991 and E/D = 0.001 for **4**, respectively (SI Figure S13). The temperature-dependent μ_{eff} of complexes **2** and **4** in the solid state decrease from 4.06 μ_B at 300 K to 2.94 μ_B at 2 K for **2** and 4.21 μ_B at 300 K to 3.21 μ_B at 2 K for **4**, respectively. The SQUID fitting shows a large zero-field splitting D = +11.7 cm^{-1} for MNIC **2** and +8.4 cm^{-1} for MNIC **4** (SI Figure S14), similar to the S = 3/2 $\{Fe(NO)\}^7$ *cis*-[(cyclam)Fe(NO)I]$^+$ with D =

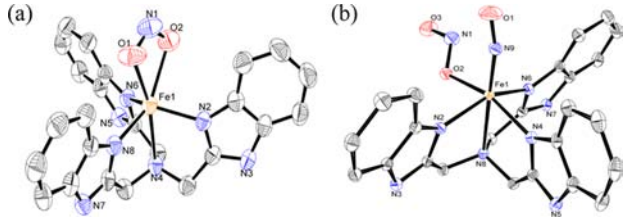

Figure 1. ORTEP drawing and labeling scheme of (a) $[(Bim)_3Fe(\kappa^2\text{-}O_2N)][BF_4]$ (**3**) and (b) $[(Bim)_3Fe(NO)(\kappa^1\text{-}ONO)][BF_4]_2$ (**4**) with thermal ellipsoid drawn at 30% probability. Selected bond lengths (Å) and angles (deg): Fe(1)−N(2) 2.111(4), Fe(1)−N(4) 2.409(4), Fe(1)−N(6) 2.100(4), Fe(1)−N(8) 2.109(4), Fe(1)−O(1) 2.104(4), Fe(1)−O(2) 2.338(4), N(1)−O(2) 1.247(6), N(1)−O(1) 1.264(7), O(1)−Fe(1)−O(2) 55.5(2) for complex **3**; Fe(1)−N(2) 2.088(1), Fe(1)−N(4) 2.128(1), Fe(1)−N(6) 2.086(1), Fe(1)−N(8) 2.378(1), Fe(1)−N(9) 1.757(2), N(9)−O(1) 1.156(2), N(1)−O(3) 1.220(2), N(1)−O(2) 1.296(2), Fe(1)−O(2) 2.063(1), Fe(1)−N(9)−O(1) 161.2(2), O(3)−N(1)−O(2) 114.7(2) for complex **4**.

dx.doi.org/10.1021/ja4105864 | J. Am. Chem. Soc. 2013, 135, 18758−18761

+12.6 cm^{-1} and $[(L)Fe(NO)(N_3)_2]$ with D = +13.6 cm^{-1} (L = 1,4,7-trimethyl-1,4,7-triazacyclononane).[29,30] In combination with magnetic susceptibility study and EPR data, the electronic structures of complexes **2** and **4** are consistent with $\{Fe^{III}(NO^-)\}^7$ system and may be described as a high spin Fe^{III} (S_{Fe} = 5/2) anti-ferromagnetically coupled with NO^- (S_{NO} = 1).[31]

To explore the coordinated-nitrite activation of [Fe^{II}-*O*,*O*-nitrito] of complex **3**, protonation of complex **3** was conducted. Interestingly, complex **3** consumes 1 equiv of AcOH/AcOD to produce nearly 1 equiv of NO gas along with the formation of $[(Bim)_3Fe(\mu\text{-}O)(\mu\text{-}OAc)Fe(Bim)_3]^{3+}$ (**5**) and H_2O/DHO (Scheme 2a and Figure 2). The EPR-silent diferric complex **5**

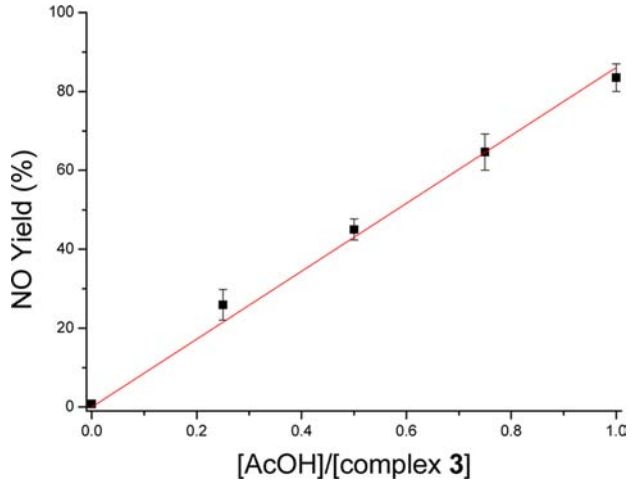

Figure 2. Plot of NO yield and the molar ratio of [AcOH]/[complex **3**]. The NO yield is calculated on the basis of the yield of $[PPN][S_5Fe(NO)_2]$, derived from the reaction of $[PPN]_2[S_5Fe(\mu\text{-}S)_2FeS_5]$ and the released NO(*g*).

and DHO were identified by UV−vis, $^1H/^2D$ NMR spectroscopies and single-crystal XRD (SI Figures S15−S18). This result is significantly different from the previous reports that two protons were needed to trigger nitrite reduction producing NO observed in the protonation of [Fe^{II}-nitro] complexes.[18,21−23,26] In order to gain more information about the formation pathway of complex **5** and NO, the reaction of complex **3** and AcOH was monitored by EPR spectroscopy. As shown in SI Figure S19, EPR spectra display the formation of complex **4** (S = 3/2, g_1 = 4.027, g_2 = 3.941, g_3 = 1.997) when complex **3** was reacted with AcOH in a 1:1 (or 1:2 and 1:10 molar ratio and stirred for 10 and 5 min, respectively) molar ratio and stirred for 20 min in MeCN at 0 °C. The formation of complex **4** was also identified by a diagnostic IR ν_{NO} at 1791 cm^{-1} in MeCN. Presumably, the facile NO-trapping property of complex **3** competitively traps the initially produced NO(*g*) to yield complex **4** when 1 equiv of AcOH was added into the MeCN solution of complex **3** to trigger the coordinated-κ^2-*O*,*O*-nitrito activation producing NO (Scheme 2b). Since the nitrosyl group of MNIC **4** is known to be easier to liberate NO to reform complex **3** via nitrito chelation (Scheme 2c), the released NO(*g*) was then trapped by $[PPN]_2[S_5Fe(\mu\text{-}S)_2FeS_5]$ to produce the known complex $[PPN][S_5Fe(NO)_2]$ (SI Experimental Section: Reaction of $[(Bim)_3Fe(\kappa^2\text{-}O_2N)][BF_4]$ (**3**) and 1 equiv of AcOH).[32] The plot of NO yield and the molar ratio of [AcOH]/[complex **3**] shows NO yield is around 84% when complex **3** is reacted with AcOH in 1:1 molar ratio in MeCN (Figure 2). Presumably, acetate ion plays a significant role in promoting the transformation of complex **3** into the acetate-bridged complex **5** upon addition of one equiv of acetic acid into MeCN solution of complex **3**. Attempts to measure the rate constant and kinetic parameters by analyzing kinetic UV−vis spectra were unsuccessful due to the overlap of the absorption bands of complex **3** with those of complexes **4** and **5**.

Density function theory (DFT) calculations with UM06 functional and 6-31G* basis sets were employed to gain insight into the mechanism of the coordinate-nitrite activation of complex **3**. Since iron-nitrito and iron-nitro complexes have been identified in biological system, both of $[Fe(\kappa^2\text{-}O_2N)]$ and $[Fe(\kappa^1\text{-}NO_2)]$ binding modes are considered as starting states to react with 1 equiv of AcOH. The results are summarized in Figure 3

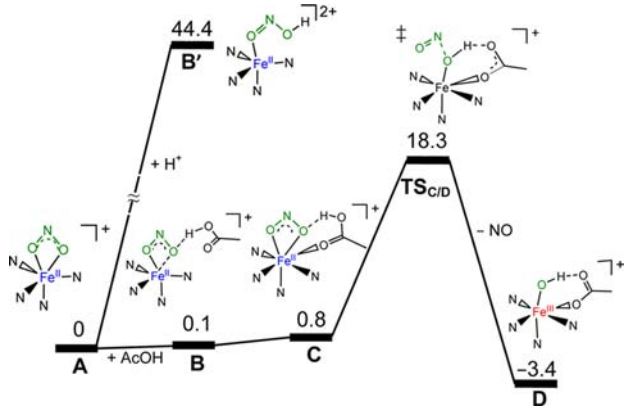

Figure 3. UM06/6-31G* free-energy profile for nitrite activation from $[(Bim)_3Fe^{II}(\kappa^2\text{-}O_2N)]$ (**A**) and 1 equiv of AcOH to $[(Bim)_3Fe^{III}(OH)(OAc)]$ (**D**) and nitric oxide. $(Bim)_3$ ligand is simplified as four N atoms.

and SI Figure S20, respectively. Although it is noted that the N-isomer is favored over the O-isomer by 6.0 kcal/mol in ferrous heme d_1 models,[33] the O-isomer $[Fe^{II}(\kappa^2\text{-}O_2N)]$ (**A**) was found to be more stable than the N-isomer $[Fe^{II}(\kappa^1\text{-}NO_2)]$ (**E**) by 7.7 kcal/mol. Presumably, it is attributed to the weaker *trans effect* of amine and electron-donating ability of the equatorial benzimidazole ligands, compared to the energy levels between N- and O-isomer in heme models with axial imidazole and equatorial porphyrin ligands.

In the [Fe-*O*,*O*-nitrito]-mediated nitrite activation (Figure 3), conformation **A** is initially associated with AcOH to form H-bonded conformation **B**. In contrast, the proton dissociation mechanism in the **A**-to-$[Fe^{II}(\kappa^1\text{-}O{=}N{-}O{-}H)]$ (**B′**) step is energy-unfavorable by 44.4 kcal/mol. In the **B**-to-**C** step, the $[Fe^{II}\cdots O{=}C(OH)CH_3]$ interaction is thermodynamically less favorable with reaction free-energy change of 0.7 kcal/mol. Conformation **C** is proposed as a ready state of nitrite reduction (SI Figure S21b). Subsequently, a proton-induced-electron transfer (PIET)[34] occurs in the **C**-to-**C′**-to-$\mathbf{TS_{C/D}}$-to-**D** step, leading to the formation of $[(Bim)_3Fe^{III}(OH)(OAc)]^+$ (**D**) and the liberation of NO molecule (Figure 3 and SI Figure S21c-e). In this PIET kinetic event, a proton transfer from AcOH to O_{endo} atom of nitrito triggers the conversion of bidentate-*O*,*O*-nitrito group of conformaiton **C** into monodentate-*O*-bound nitrous acid of conformation **C′** $[Fe^{II}(\kappa^1\text{-}OH(N{=}O)]$ (SI Figure S21c). An electron transfer from the iron(II) to the nitrito then occurs to result in the cleavage of the $N{-}O_{endo}$ bond and the release of NO, as shown in SI Figure S22. The decrease of the $Fe\cdots O_{acetate}$ distance (from 2.307 Å in **C** to 1.986 Å in $\mathbf{TS_{C/D}}$ and to 1.970 Å in **D**) rationalizes the stabilizing interaction between iron and

dx.doi.org/10.1021/ja4105864 | J. Am. Chem. Soc. 2013, 135, 18758−18761

acetate (SI Figure S21). The **C**-to-$\mathbf{TS}_{C/D}$-to-**D** transformation is found to have an activation free energy of 17.5 kcal/mol and a reaction free energy of −4.2 kcal/mol (Figure 3). Conformation **D** compounds are proposed to dimerize to yield complex **5** accompanied by the release of one acetate and one water molecule.

In contrast, the mechanism of [Fe-nitro]-mediated nitrite activation may be ruled out (SI Figure S20). In the [Fe-nitro] models, conformation **E** is initially associated with AcOH to yield energy-favorable conformation **F** by −6.1 kcal/mol, followed by a proton transfer to form conformation **G**. However, OH^- releases along with conversion of **G** into **H** is severely energy-unfavorable by 88.8 kcal/mol. Also, the proton dissociation product $[Fe^{II}(\kappa^1\text{-}N(=O)(OH)]$ (**F′**) is energy-unfavorable by 34.9 kcal/mol.

In summary, transformation of the paramagnetic *O*,*O*-nitrito-bound complex **3** into EPR-silent diferric complex **5** along with the release of NO(*g*) and H_2O triggered by AcOH (1:1 molar ratio) demonstrates that *O*,*O*-nitrito-containing complex **3** serves as an intermediary for the conservation of NO, and $[(Bim)_3Fe^{II}]$ motif acts as an active center to regulate the transformation of nitrite into NO via a proton-induced-electron transfer mechanism. This finding may not only support a possible protonation pathway for deoxyhemoglobin-/deoxyhemerythrin-mediated nitrite activation (study of reaction of complex **3** and other acids is undergoing), but it also provides a new type of nitrite-reduction to nitric oxide in model chemistry.

■ ASSOCIATED CONTENT

Ⓢ Supporting Information

IR, UV−vis, EPR, ^{1}H NMR, ^{2}D NMR spectra, SQUID, crystallographic, computational details and experimental section. This material is available free of charge via the Internet at http://pubs.acs.org.

■ AUTHOR INFORMATION

Corresponding Author

wfliaw@mx.nthu.edu.tw

Notes

The authors declare no competing financial interest.

■ ACKNOWLEDGMENTS

We gratefully acknowledge financial support from the National Science Council of Taiwan. We also thank National Center for High-Performance Computing (NCHC) for their support on the hardware and software applied in this work. Authors thank Mr. Ting-Shen Kuo and Mrs. Pei-Lin Chen for the single-crystal X-ray structural determinations, and Dr. I-Jui Hsu, Dr. Hsing-Yin Chen, Dr. Li-Kang Chu and Dr. Yun-Wei Chiang for helpful discussion.

■ REFERENCES

(1) Lundberg, J. O.; Weitzberg, E.; Gladwin, M. T. *Nat. Rev. Drug Discovery* **2008**, *7*, 156.
(2) Heinecke, J.; Ford, P. C. *Coord. Chem. Rev.* **2010**, *254*, 235.
(3) Xu, N.; Yi, J.; Richter-Addo, G. B. *Inorg. Chem.* **2010**, *49*, 6253.
(4) Yi, J.; Thomas, L. M.; Richter-Addo, G. B. *Angew. Chem., Int. Ed. Engl.* **2012**, *51*, 3625.
(5) Yi, J.; Heinecke, J.; Tan, H.; Ford, P. C.; Richter-Addo, G. B. *J. Am. Chem. Soc.* **2009**, *131*, 18119.
(6) Yi, J.; Safo, M. K.; Richter-Addo, G. B. *Biochemistry* **2008**, *47*, 8247.
(7) Cosby, K.; Partovi, K. S.; Crawford, J. H.; Patel, R. P.; Reiter, C. D.; Martyr, S.; Yang, B. K.; Waclawiw, M. A.; Zalos, G.; Xu, X.; Huang, K. T.; Shields, H.; Kim-Shapiro, D. B.; Schechter, A. N.; Cannon, R. O., 3rd; Gladwin, M. T. *Nat. Med.* **2003**, *9*, 1498.
(8) Doyle, M. P.; Pickering, R. A.; DeWeert, T. M.; Hoekstra, J. W.; Pater, D. *J. Biol. Chem.* **1981**, *256*, 12393.
(9) Huang, K. T.; Keszler, A.; Patel, N.; Patel, R. P.; Gladwin, M. T.; Kim-Shapiro, D. B.; Hogg, N. *J. Biol. Chem.* **2005**, *280*, 31126.
(10) Perissinotti, L. L.; Marti, M. A.; Doctorovich, F.; Luque, F. J.; Estrin, D. A. *Biochemistry* **2008**, *47*, 9793.
(11) Reddy, D.; Lancaster, J. R., Jr.; Cornforth, D. P. *Science* **1983**, *221*, 769.
(12) Zhang, W.-X.; Xu, M.-S.; Wang, G.-H.; Wang, M.-Y. *Cancer Res.* **1983**, *43*, 339.
(13) Glidewell, C.; Glidewell, S. M. *Food Chem.* **1993**, *46*, 225.
(14) Nocek, J. M.; Kurtz, D. M., Jr.; Pickering, R. A.; Doyle, M. P. *J. Biol. Chem.* **1984**, *259*, 12334.
(15) Khin, C.; Heinecke, J.; Ford, P. C. *J. Am. Chem. Soc.* **2008**, *130*, 13830.
(16) Kurtikyan, T. S.; Hovhannisyan, A. A.; Iretskii, A. V.; Ford, P. C. *Inorg. Chem.* **2009**, *48*, 11236.
(17) Heinecke, J.; Ford, P. C. *J. Am. Chem. Soc.* **2010**, *132*, 9240.
(18) Ching, W.-M.; C.-H., C.; Wu, C.-W.; Peng, C.-H.; Hung, C.-H. *J. Am. Chem. Soc.* **2009**, *131*, 7952.
(19) Patra, A. K.; Afshar, R. K.; Rowland, J. M.; Olmstead, M. M.; Mascharak, P. K. *Angew. Chem., Int. Ed. Engl.* **2003**, *42*, 4517.
(20) Afshar, R. K.; Eroy-Reveles, A. A.; Olmstead, M. M.; Mascharak, P. K. *Inorg. Chem.* **2006**, *45*, 10347.
(21) Villar-Acevedo, G.; Nam, E.; Fitch, S.; Benedict, J.; Freudenthal, J.; Kaminsky, W.; Kovacs, J. A. *J. Am. Chem. Soc.* **2011**, *133*, 1419.
(22) Harris, T. D.; Betley, T. A. *J. Am. Chem. Soc.* **2011**, *133*, 13852.
(23) López, J. P.; Heinemann, F. W.; Prakash, R.; Hess, B. A.; Horner, O.; Jeandey, C.; Oddou, J.-L.; Latour, J.-M.; Grohmann, A. *Chem.—Eur. J.* **2002**, *8*, 5709.
(24) Enemark, J. H.; Feltham, R. D. *Coord. Chem. Rev.* **1974**, *13*, 339.
(25) Tsai, F.-T.; Kuo, T.-S.; Liaw, W.-F. *J. Am. Chem. Soc.* **2009**, *131*, 3426.
(26) Tsai, F.-T.; Chen, P.-L.; Liaw, W.-F. *J. Am. Chem. Soc.* **2010**, *132*, 5290.
(27) Tsai, F. T.; Lee, Y. C.; Chiang, M. H.; Liaw, W. F. *Inorg. Chem.* **2013**, *52*, 464.
(28) Rodionov, V. O.; Presolski, S. I.; Gardiner, S.; Lim, Y.-H.; Finn, M. G. *J. Am. Chem. Soc.* **2007**, *129*, 12696.
(29) Hauser, C.; Glaser, T.; Bill, E.; Weyhermüller, T.; Wieghardt, K. *J. Am. Chem. Soc.* **2000**, *122*, 4352.
(30) Brown, C. A.; Pavlosky, M. A.; Westre, T. E.; Zhang, Y.; Hedman, B.; Hodgson, K. O.; Solomon, E. I. *J. Am. Chem. Soc.* **1995**, *117*, 715.
(31) Li, M.; Bonnet, D.; Bill, E.; Neese, F.; Weyhermüller, T.; Blum, N.; Sellmann, D.; Wieghardt, K. *Inorg. Chem.* **2002**, *41*, 3444.
(32) Tsai, M.-L.; Chen, C.-C.; Hsu, I-J.; Ke, S.-C.; Hsieh, C.-H.; Chiang, K.-A.; Lee, G.-H.; Wang, Y.; Liaw, W.-F. *Inorg. Chem.* **2004**, *43*, 5159.
(33) Silaghi-Dumitrescu, R. *Inorg. Chem.* **2004**, *43*, 3715.
(34) Ghosh, S.; Dey, A.; Sun, Y.; Scholes, C. P.; Solomon, E. I. *J. Am. Chem. Soc.* **2009**, *131*, 277.